Spallarossa, D., Kotha, S. R., Picozzi, M., Barani, S., Bindi, D. (2019): On-site Earthquake Early Warning: a partially non-ergodic perspective from the site effects point of view. - *Geophysical Journal International*, *216*, 2, pp. 919—934.

DOI: http://doi.org/10.1093/gji/ggy470

Geophysical Journal International

Geophys. J. Int. (2019) **216,** 919–934
Advance Access publication 2018 November 10
GJI Seismology

doi: 10.1093/gji/ggy470

On-site earthquake early warning: a partially non-ergodic perspective from the site effects point of view

D. Spallarossa,[1] S.R. Kotha,[2] M. Picozzi,[3] S. Barani[1] and D. Bindi[2]

[1] *University of Genova - DISTAV, Dipartimento di Scienza della Terra, dell'Ambiente e della Vita, Corso Europa 26, 16132 Genoa, Italy*
[2] *Helmholtz Centre Potsdam, GFZ German Research Centre for Geosciences, Telegrafenberg 14473, Potsdam, Germany. E-mail: bindi@gfz-potsdam.de*
[3] *University of Naples Federico II, Dipartimento di Fisica, via Cinthia 21, 80126 Naples, Italy*

Accepted 2018 November 6. Received 2018 November 4; in original form 2018 July 31

SUMMARY

We introduce in the on-site earthquake early warning (EEW) a partially non-ergodic perspective from the site effects point of view. We consider the on-site EEW approach where the peak ground velocity (PGV) for *S* waves is predicted from an early estimate, over the *P* waves, of either the peak-displacement (PD) or cumulative squared velocity (IV2). The empirical PD-PGV and IV2-PGV relationships are developed by applying a mixed-effect regression where the site-specific modifications of ground shaking are treated as random effects. We considered a large data set composed of almost 31 000 selected recordings in central Italy, a region struck by four earthquakes with magnitude between 6 and 6.5 since the 2009 L'Aquila earthquake. We split the data set into three subsets used for calibrating and validating the on-site EEW models, and for exemplifying their application to stations installed after the calibration phase. We show that the partially non-ergodic models improve the accuracy of the PGV predictions with respect to ergodic models derived for other regions of the world. Moreover, considering PD and accounting for site effects, we reduce the (apparent) aleatory variability of the logarithm of PGV from 0.31 to 0.36, typical values for ergodic on-site EEW models, to about 0.25. Interestingly, a lower variability of 0.15 is obtained by considering IV2 as proxy, which suggests further consideration of this parameter for the design of on-site EEW systems. Since being site-specific is an inherent characteristic of on-site EEW applications, the improved accuracy and precision of the PGV predicted for a target protection translate in a better customization of the alert protocols for automatic actions.

Key words: earthquake early warning; earthquake ground motion; site effects.

1 INTRODUCTION

In the framework of earthquake early warning (EEW), one of the most modern and technological response of society to seismic risk, the on-site (or single station) approach refers to the strategy of promptly delivering to targets real-time alert messages containing information on the *S* waves ground shaking predicted by measurements taken over the early *P*-wave window. In the case of the on-site EEW, hence, users or automatic devices can exploit the time difference between the early *P* wave and the following *S* waves arrival at the seismic station (i.e. the lead-time) to undertake actions mitigating their exposure to seismic risk. Contrariwise, in the regional approach a strong motion network is installed close to a seismogenic area and used for the rapid detection and characterization (e.g. in terms of magnitude and location) of the occurred earthquake again exploiting early *P*-waves signals (Satriano *et al.* 2011; Picozzi *et al.* 2015). Whenever a target is located at a distance larger than the one traveled by the *S* waves during the time spent for estimating the event location and magnitude from *P* waves, users can benefit from a certain amount of lead-time. The selection of approaches to design a specific EEW system will therefore depend on both technological (i.e. essentially the software and telemetry speed) and geometrical (i.e. the distance between the known seismic threats and the targets) considerations. Whenever a seismic network is not equipped with a telemetry system suitable for EEW operations (i.e. delay in data transmission equals to or smaller than 1 s), or the target to secure is located within the so called blind zone of a regional EEW network (i.e. the ground shaking at the target cannot be predicted before the arrival of *S* wave due to the short epicentral distance), the on-site approach is the best possible choice, as the station is

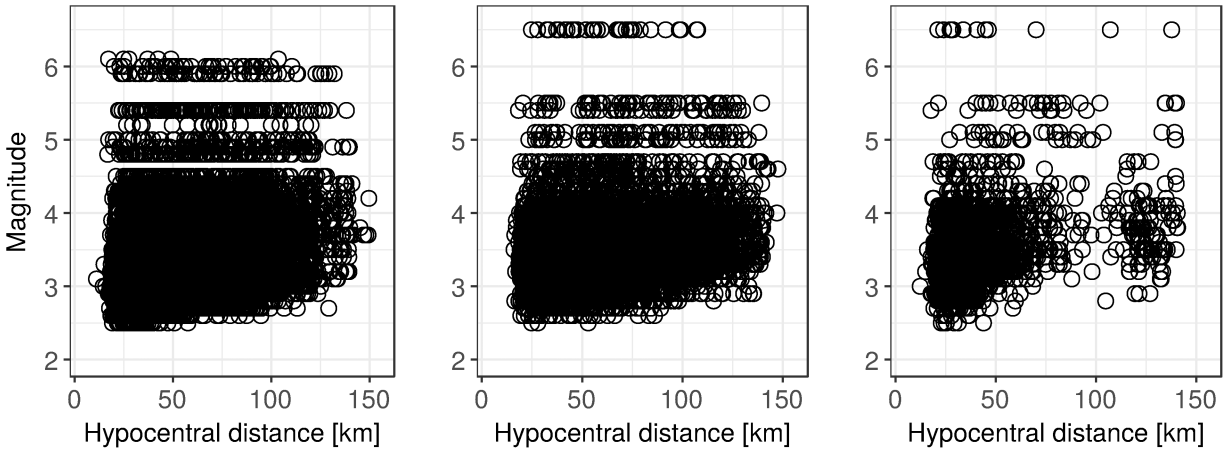

Figure 1. Magnitude versus hypocentral distance scatter plot for D_{cal} (left), D_{val} (middle) and D_{app} (right). For the purpose of this figure, the moment magnitude is used when available, otherwise the local magnitude is considered. The locations of the Istituto Nazionale di Geofisica and Vulcanologia-INGV seismic bulletin (http://cnt.rm.ingv.it/) are considered for computing the distances.

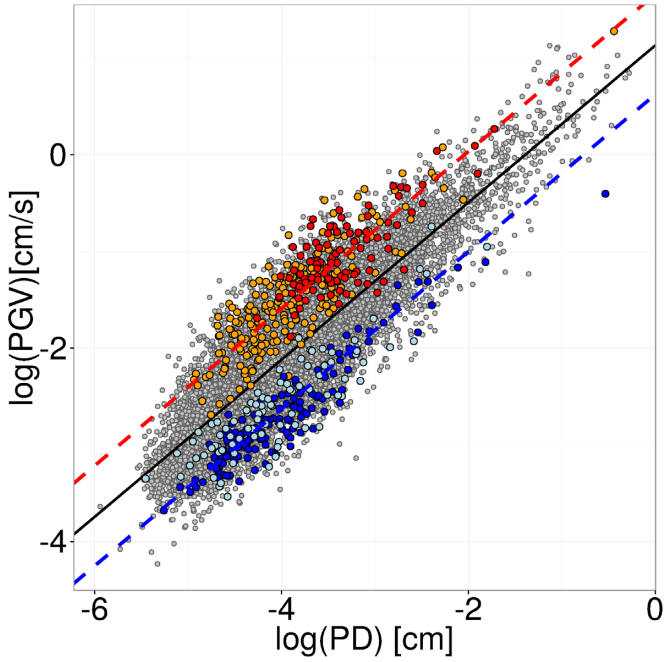

Figure 2. Comparison between the distribution of the observed PGV versus PD (grey circles), condidering D_{cal}, and the average predictions (black line) from the model reported in Table 2. Observations from stations NCR, T1243, SACS and PTQR are shown in red, orange, blue and cyan, respectively. The predictions accounting for $\delta P2S$ are shown as red and blue dashed lines for stations NCR and SACS, respectively.

located in the proximity of the target site (Zollo *et al.* 2010; Bindi *et al.* 2016). On-site approaches rely on the application of empirical relationships calibrated over past earthquakes that relate the ground shaking associated with the early *P* waves, for example, in terms of peak ground displacement (PD, Wu *et al.* 2006; Zollo *et al.* 2006) or the cumulative squared velocity (IV2, Festa *et al.* 2008), to the corresponding shaking associated with the *S* waves (e.g. in terms of peak ground velocity, PGV). Different studies proposed empirical relationships for on-site EEW (Kanamori 2005; Wu & Kanamori 2008; Böse *et al.* 2009; Zollo *et al.* 2010; Picozzi 2012; Brondi *et al.* 2015; Colombelli *et al.* 2015; Caruso *et al.* 2017). The data sets used for the calibration generally include recordings from multiple stations in a given region, such as (Caruso *et al.* 2017) for Italy; (Wu & Kanamori 2005) for Taiwan; (Wu *et al.* 2006) for California, or include data from different regions (Wu *et al.* 2006; Zollo *et al.* 2010). Generally, empirical relationships are calibrated without considering the station-to-station variability (Wang & Wu 2014), thus incorporating the response of the installation site into the ground motion aleatory variability. Following recent advances in PSHA (Atkinson 2006; Rodríguez-Marek *et al.* 2013; Kotha *et al.* 2017), ground

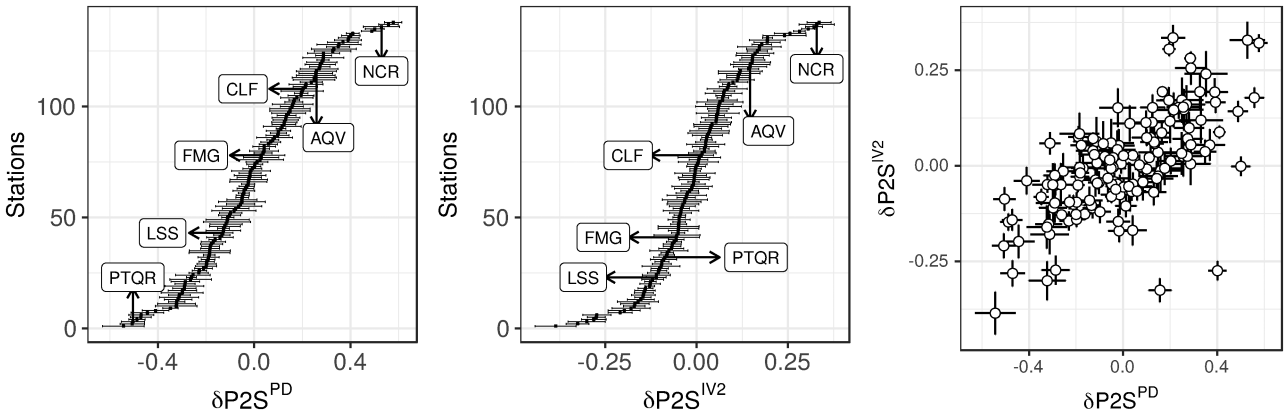

Figure 3. Station-to-station residuals $\delta P2S$ for stations in the calibration data set D_{cal}, considering PD (left) and IV2 (middle). For each station, the mean $\delta P2S$ (black square) and its 95 per cent confidence interval (horizontal bar) are shown and the values for a few selected stations indicated with labels. In the right panel, the $\delta P2S$ values obtained for PD and IV2 are compared.

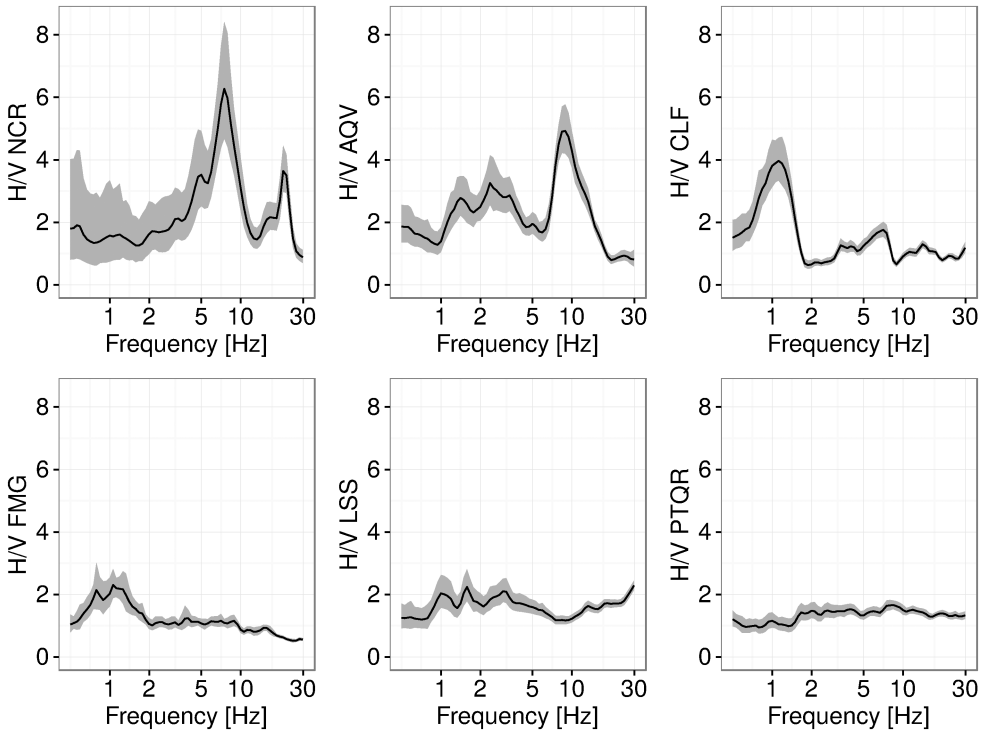

Figure 4. Horizontal to vertical spectral ratio (H/V) for 6 stations whose $\delta P2S$ are indicated in Fig. 3. Each panel shows the mean logarithm spectral ratio (black) and the corresponding ± 1 standard deviation interval (grey ribbon). The geometric mean of the two horizontal components is considered.

motion estimates can be improved through identification and quantification of site effects; that is, by relaxing the so-called ergodic assumption (Anderson & Brune 1999). The aim of this study is to import the methodology developed in the PSHA framework within the on-site EEW one, and in particular to refine the development of on-site EEW relationships by including site specific amplification factors in the models. We follow the approach used in partially non-ergodic probabilistic seismic hazard assessment (Anderson & Brune 1999): site-specific amplifications (or de-amplifications) are isolated from the residual distribution, and the relevant site-to-site variability removed from the aleatory variability (Abrahamson & Hollenback 2012). We apply the procedure in central Italy, a region struck by four earthquakes with moment magnitude above 6 since the 2009 L'Aquila earthquake (Chiaraluce *et al.* 2017). We first describe the set of recordings used to calibrate the site specific on-site EEW models. Then, the models are validated using recordings from independent earthquakes, considering the cases where the station corrections are either known or unknown. In the latter case, a procedure for estimating the site corrections is discussed. Finally, the improvement achieved by considering the site-specific models is discussed with respect to the results obtained using both the the standard ergodic approach and relationships developed in other studies.

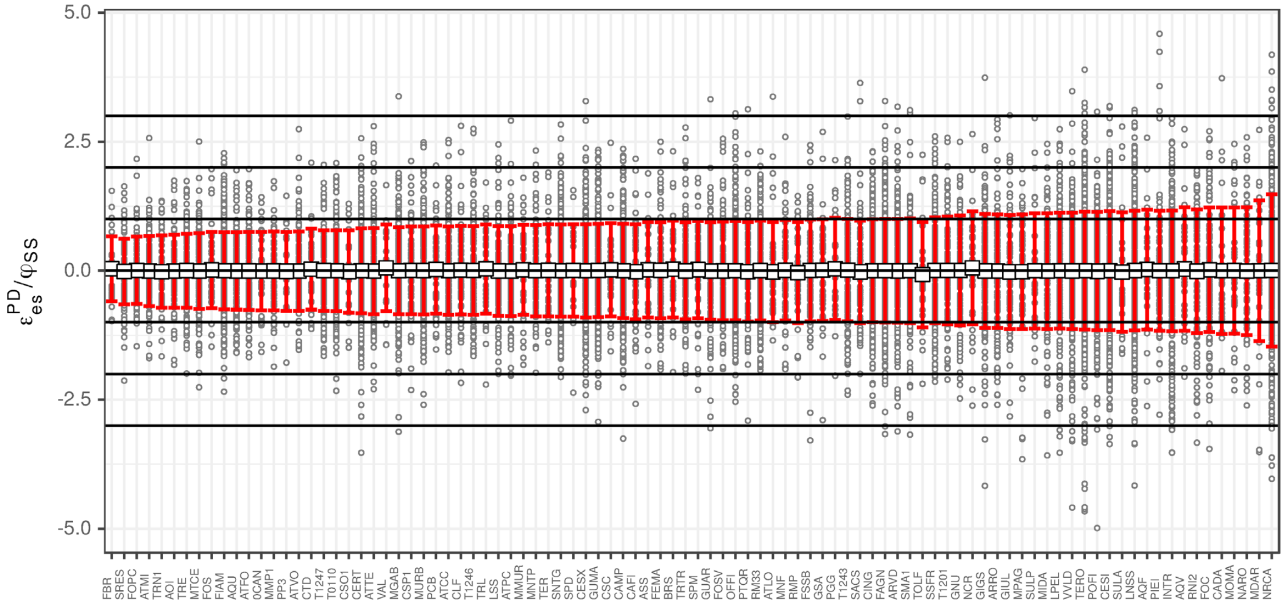

Figure 5. Residuals ϵ_{es}^{PD} normalized to ϕ_{SS} (circles) grouped for stations in D_{cal}. For each station, the mean normalized residual (white square) and the normalized single-station variability $\phi_{SS,\,s}/\phi_{SS}$ (vertical red bars) are shown. The horizontal lines correspond to $\pm1\phi_{SS}$, $\pm2\phi_{SS}$ and $\pm3\phi_{SS}$.

2 DATA

The data set considered in this study is composed by 83 237 recordings in the magnitude range 2.5–6.5, hypocentral distances from 10 to 150 km, and generated by 1902 earthquakes occurred in central Italy between 2008 and 2018. In the following, we provide the reader with a brief description of the data set. A detailed description can be found in (Bindi *et al.* 2018).

All data were collected from the National Seismic Network (RSN), the Mediterranean Network (Mednet), the Rapid Response Network operated by the Istituto Nazionale di Geofisica e Vulcanologia (INGV) and the National Accelerometric Network (RAN) operated by the Department of Civil Protection (DPC). Except for the data from the DPC repository (http://ran.protezionecivile.it/IT/index.php), the waveforms were retrieved from the European Integrated Data Archive (https://www.orfeus-eu.org/data/eida/). All recordings underwent instrumental correction, including the application of a pre-deconvolution Butterworth bandpass filter with an adaptive high-pass corner-frequency spanning the range 0.05–0.4 Hz, depending on the signal-to-noise ratio (SNR), and a low-pass corner frequency fixed to 40 Hz. Strong motion data from the the DPC repository were processed following the procedure of the Italian strong motion data base ITACA (Luzi *et al.* 2008; Paolucci *et al.* 2011). Only recordings with SNR greater than 6 for at least 75 per cent of the frequencies within the frequency range were considered in the analysis. For each processed recording, we computed the integral of the squared velocity (*IV*2) (Kanamori *et al.* 1993; Brondi *et al.* 2015) and the peak ground displacement (*PD*) over the vertical *P*-wave window (i.e. considering a time window starting from the *P*-wave onset and ending at the *S*-wave arrival). Following (Picozzi *et al.* 2017), the *PD* was computed after application of a bandpass filter 0.075–3.0 Hz. Moreover, we computed the *S*-wave peak ground velocity (*PGV*) as the geometrical mean of the values relative to the two horizontal components. To develop the on-site EEW models, we considered a data set including 175 stations with at least 20 recordings covering a hypocentral distance range of at least 25 km and a magnitude range spanning at least 2 magnitude units. The data set selected for the analysis is composed by 31 000 recordings.

The selected data set was split into three separate data sets (Figs 1 and A1): DS_{cal}, DS_{val} and DS_{app}. In the following, we refer to DS_{cal} as the calibration data set. It is composed of 16 478 recordings from 872 earthquakes occurred before 2016 October 29 and recorded by 138 stations. The validation data set DS_{val} includes 12 018 recordings from 501 earthquakes occurred after 2016 October 29 and recorded by 94 stations shared with DS_{cal}. Finally, the data set DS_{app} is completely disjoint from DS_{cal} since it includes 2333 recordings from 443 earthquakes occurred after 2016 October 29, recored by 37 stations not belonging to DS_{cal}. Moreover, DS_{cal} includes *PD* and *IV*2 values in the range $[10^{-6} - 0.5]$ cm and $[10^{-10} - 4]$ cm^2 s^{-1}, respectively, corresponding to *PGV* in the range $[6\,10^{-5} - 13.4]$ cm s^{-1}; DS_{val} includes *PD* and *IV*2 values in the range $[2.5\,10^{-6} - 0.98]$ cm and $[10^{-10} - 5.7]$ cm^2 s^{-1}, respectively, corresponding to *PGV* in the range $[8–10^{-5} - 36.4]$ cm s^{-1}. The spatial distribution of stations and events of the three data sets is shown in Fig. A1 of the Appendix.

3 MODEL CALIBRATION

The relationships relating the logarithm (in base 10) of the *S*-wave peak ground velocity *PGV* to an early estimate (i.e. over *P* waves) of the logarithm of either the peak displacement (*PD*) or the integral of the squared-velocity (*IV*2) are obtained by performing a mixed-effects regression (Pinheiro & Bates 2000; Bates *et al.* 2015) over D_{cal}

$$Log\,PGV_{es} = a_1 + a_2 \log PD_{es} + \delta P2S_s^{PD} + \delta B_e^{PD} + \epsilon_{es}^{PD} \quad (1)$$

$$Log\,PGV_{es} = b_1 + b_2 \log IV2_{es} + \delta P2S_s^{IV2} + \delta B_e^{IV2} + \epsilon_{es}^{IV2}, \quad (2)$$

where the coefficients a_i and b_i, with $i = 1, 2$, define the median predictions (fixed effects); $\delta P2S_s^{type}$, δB_e^{type}, with *type* either *PD* or *IV*2 are the random effects (normal distributions with zero mean) describing the station-to-station and the between-event residuals,

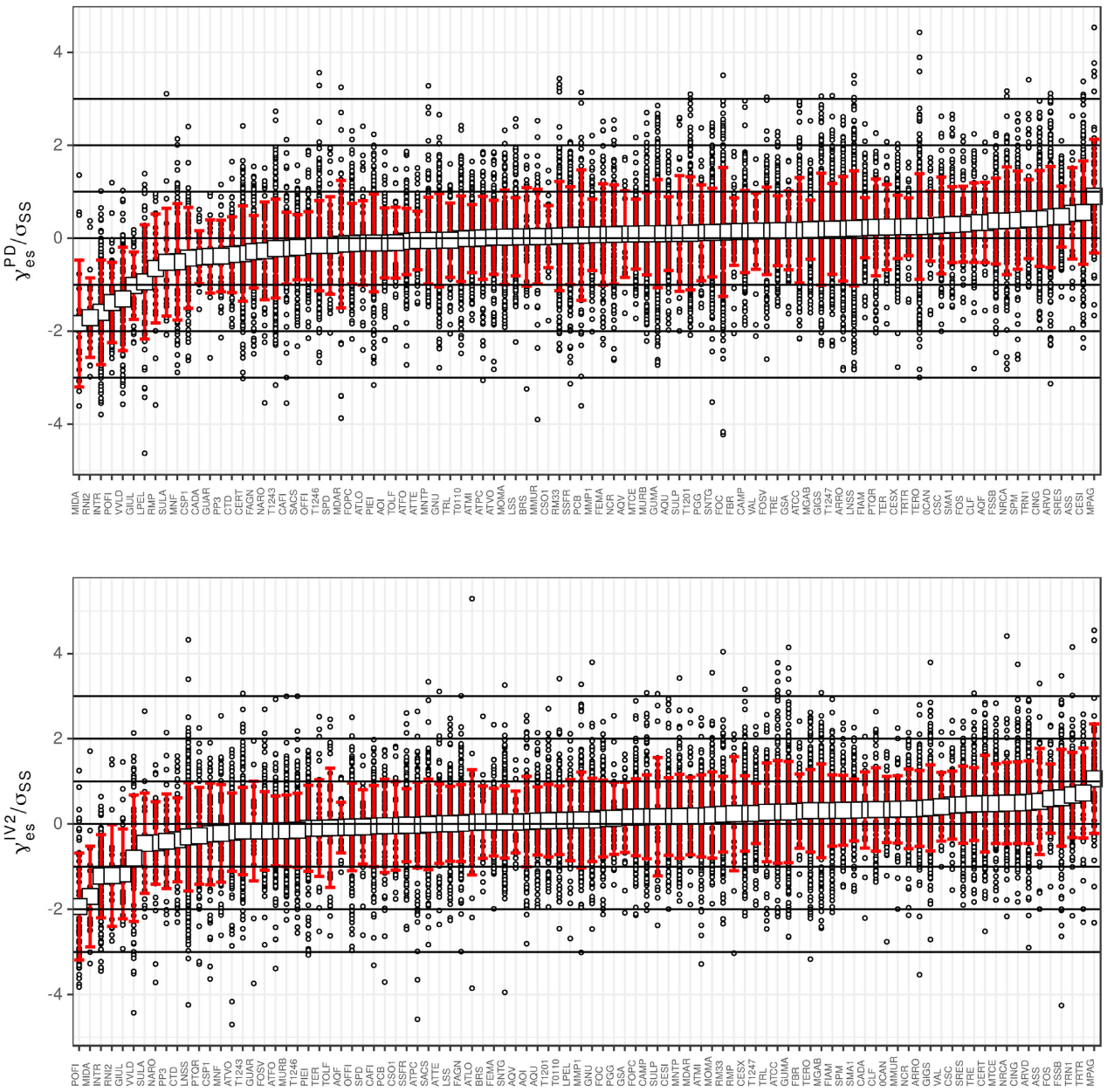

Figure 6. Residuals γ_{es} (see eqs 4 and 5) normalized to σ_{SS} (circles) grouped for stations in D_{val}, considering *PD* (top) and *IV*2 (bottom). For each station, the mean normalized residual (white square) and the normalized single-station variability $\phi_{SS,s}/\sigma_{SS}$ (vertical red bars) are shown. The horizontal lines correspond to $\pm 1\sigma_{SS}$, $\pm 2\sigma_{SS}$ and $\pm 3\sigma_{SS}$.

respectively, for station s and event e; ϵ_{es}^{type} indicates the event- and station-corrected residual, also referred to as single-station within-event residuals, δWS_{es} (Al Atik *et al.* 2010). In the following, we drop the usage of the superscript *type* when referring to the generic distribution. The standard deviations of the normal distributions of $\delta P2S$, δB and ε are indicated with ϕ_{P2S}, τ and ϕ_{SS}, respectively. The standard deviation of the models is given by $\sigma = \sqrt{\phi_{P2S}^2 + \tau^2 + \phi_{SS}^2}$ and quantifies the (apparent) aleatory variability of the models. For reader convenience, the above nomenclature, which is a de-factor standard in the analysis of the ground motion variability (Al Atik *et al.* 2010), is summarized in Table 1. Aim of this study is to relax the ergodic assumption by considering the station-to-station term in computing the predictions and, consequently, by removing the corresponding variance ϕ_{P2S}^2 from the (apparent) aleatory variability σ.

The obtained coefficients a_i and b_i of models (1) and (2) are listed in Table 2. Fig. 2 compares the best fit model with the distribution of the observed PGV versus PD values. The PGV for stations NCR (red), T1243 (orange), SACS (blue) and PTQR (cyan) highlights the large contribution of the site effects to the overall PGV variability, as quantified by the distribution of the random effects for all stations listed in Table A1 of the Appendix and shown in Fig. 3. For example, the difference $\delta P2S_{NCR}^{PD} - \delta P2S_{PTQR}^{PD}$ is 1.03, corresponding to more than a factor 10 on PGV. The site effects for few selected stations are exemplified in Fig. 4, where the average horizontal-to-vertical spectral ratios (H/V) (Lermo & Chávez-García 1993) are shown. The analysis of the site effects at some of these stations was the target of previous studies. For example, station Nocera (NCR), which is classified as class E of Eurocode-8 (CEN 2004), i.e., soil

Table 1. Residual components and corresponding standard deviations. For details, see (Al Atik *et al.* 2010).

Symbol	Description
δB_e	between-events residuals δB for event e
$\delta P2S_s$	on-site EEW site-to-site residuals $\delta P2S$ for station s
ε_{es}	event and station corrected residuals ε for event e and station s (single-station within-event residuals)
τ	standard deviation of the between-events residuals
ϕ_{SS}	standard deviation of the event and station corrected residuals (standard deviation of the single-station within-event residuals)
$\phi_{SS,\,s}$	standard deviation of the event and station corrected residuals for station s
ϕ_{P2S}	standard deviation of the on-site EEW site-to-site residuals
σ_{SS}	aleatory variability of the ground motion under the partially non-ergodic single-site assumption
σ	aleatory variability of the ground motion under the ergodic assumption

Table 2. Coefficients and standard deviations of models in eqs (1) and (2). Intercept indicates coefficients a_1 and b_1; slope indicates coefficients a_2 and b_2.

Equation	Proxy	Intercept	Slope	ϕ_{P2S}	τ	ϕ_{SS}
1	PD	1.129	0.813	0.249	0.122	0.224
2	IV2	0.882	0.518	0.130	0.056	0.146

deposits with thickness smaller than about 20 m having an average shear wave smaller than 360 m/s and overlying a rock, shows strong amplifications at 7.4 and 21 Hz. Previous studies (Rovelli *et al.* 2002; Cultrera *et al.* 2003) investigated the complexities of the amplifications at Nocera, showing their dependence on the source azimuth due to the presence of a nearby fault zone. Other examples shown in Fig. 4 are Colfiorito station (CLF), installed within a basin where local induced surface waves generate strong amplification at 1 Hz (Di Giulio *et al.* 2003), and station L'Aquila-Valle Aterno (AQV), installed in the middle of the Aterno valley and showing a broad range of amplification over the frequency band 1–4 Hz and a strong peak of amplification at 10 Hz (Akinci *et al.* 2010). Such amplifications are reflected in the large $\delta P2S$ values for these three stations (Fig. 3). It is worth mentioning that the site amplifications at these stations can involve amplifications also over the vertical components (Parolai & Richwalski 2004). Therefore, $\delta P2S$ is not only an empirical estimate of the site effects affecting S waves (at those frequencies mostly contributing to PGV) which can generate, at a given station, systematic deviations from the generic PGV predictions. Indeed, $\delta P2S$ is also influenced by amplifications on the vertical components occurring at frequencies influencing either PD or IV2. In other words, the values of $\delta P2S$ for two stations with identical amplification effects on the horizontal components could be different if the two stations experience different amplifications on the vertical component. Finally, stations Pietraquaria (PTQR) and Leonessa (LSS), both installed on rock without significant amplification (Fig. 4), show large negative $\delta P2S$ values.

The $\delta P2S$ of the six stations in Fig. 4 are indicated in the distributions shown in Fig. 3. Since the $\delta P2S$ term accounts for the site-specific amplification of PGV, the $\delta P2S$ values for PD and IV2 show an overall correlation but with a large spread (right-hand panel of Fig. 3) since the frequency-dependent amplifications of the vertical component can affect differently PD or IV2 (since the former is a peak parameter in displacement, while the latter is an integral parameter in velocity).

4 SINGLE-STATION EVENT-CORRECTED RESIDUALS

The event- and station-corrected residuals ε_{es} (eqs 1 and 2) for earthquake e recorded at station s are used to compute the single station variability, which is defined as the standard deviation of the ε_{es} values grouped by station, that is:

$$\phi_{SS,s} = \sqrt{\frac{\sum_{i=1}^{N_s} \epsilon_{is}^2}{N_s - 1}}, \tag{3}$$

where the summation is performed over the N_s recordings available for station s. For the considered on-site EEW models, the standard deviation in eq. (3) represents a lower bound for the variability of the predictions computed at any specific station. The results for PD are shown in Fig. 5, where the ε_{es} values are normalized to ϕ_{SS} (i.e. the standard deviations of the overall event- and station-corrected residual ε, see Table 1). Fig. 5 shows that, when considered individually, almost all stations are characterized by a variability of residuals with respect to their own median model, $\phi_{SS,\,s}$, close to the one computed for all stations together, ϕ_{SS} (the latter corresponding to the horizontal lines at ± 1) reported in Table 2. In other words, most of the stations included in D_{cal} shows a similar variability of the single station within-event residuals. The only stations with $\phi_{SS,\,s}$ exceeding 1.25 times ϕ_{SS} are NRCA (Norcia, 307 used recordings) and MDAR (Monte Daria, 33 recordings used), located in Fig. 5 at the extreme right of the distribution. A similar distribution is obtained for *IV*2 (Fig. A2 in the Appendix) but, in this case, the two stations showing the largest variability are OFFI and ATLO.

5 MODEL VALIDATION

The recordings in the validation data set, DS_{val}, are used to test the accuracy of the models listed in Table 2. DS_{val} includes 94 stations used also for the calibration. Therefore, an estimate of $\delta P2S$ for these stations is available. The validation is performed considering about 12 000 records of earthquakes that were not included in the calibration data set DS_{cal}. The comparison between the PGV_{es} observed for earthquake e at station s and the relevant predictions is performed in terms of station-corrected residuals γ_{es}, that is

$$\gamma_{es} = Log(PGV_{es}) - a_1 - a_2\, logPD_{es} - \delta P2S_s^{PD} \tag{4}$$

and

$$\gamma_{es} = Log(PGV_{es}) - b_1 - b_2\, logIV2_{es} - \delta P2S_s^{IV2} \tag{5}$$

Since the δB_e values for these earthquakes are not known, the between event variability τ is considered in the aleatory variability and $\sigma_{SS} = \sqrt{\tau^2 + \phi_{SS}^2}$ is used to normalize γ_{es}, being σ_{SS} equal to 0.255 and 0.156 for PD and IV2, respectively. The results are shown in Fig. 6, where the stations are ordered for increasing average normalized residuals (i.e. the most anomalous stations are located in the tails of the distribution). For *PD*, most of the stations have an average γ_s (white square in Fig. 6) close to zero. Only for six stations, the average γ_s exceeds σ_{SS} (i.e. the average normalized residual γ_{es}/σ_{SS} is smaller than –1 for stations MIDA, RNI2, INTR, POFI, VVLD, GIUL), and for no stations it is larger than two times σ_{SS}, confirming that the calibrated models have a satisfactory predictive power. Similar results are obtained also for *IV*2, being $\gamma_{es}/\sigma_{SS} <$

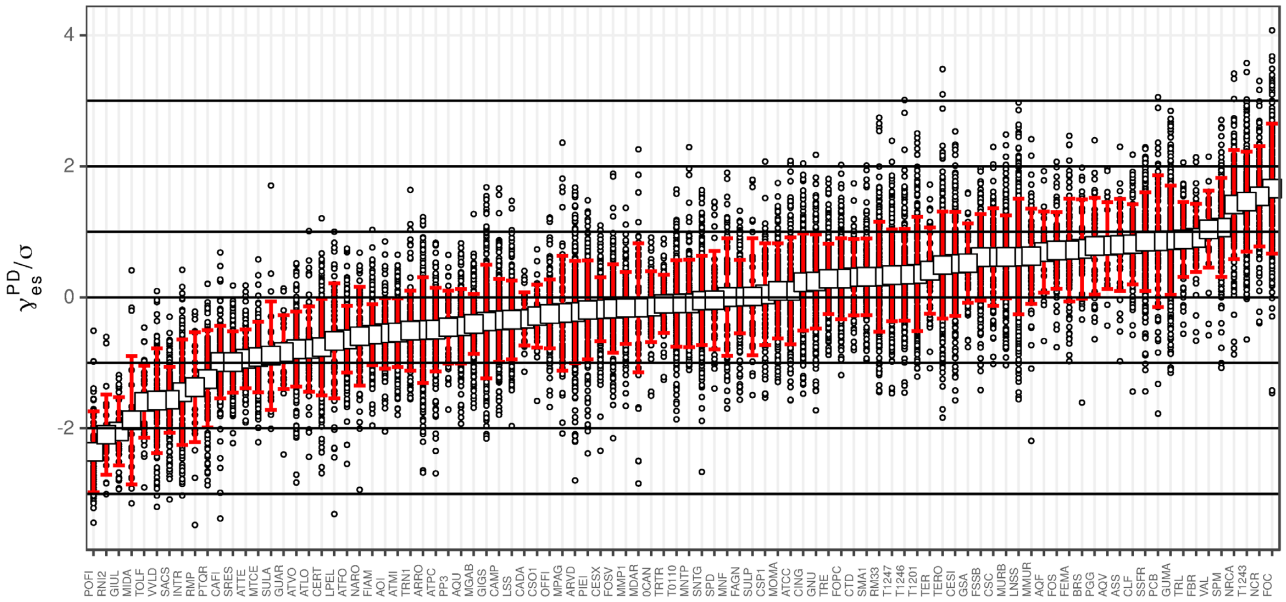

Figure 7. Residuals γ_{es} for *PD* normalized to σ (circles) grouped for stations in D_{val} without considering $\delta P2S$. For each station, the mean normalized residual (white square) and the normalized single-station variability $\phi_{SS,s}/\sigma$ (vertical red bars) are shown. The horizontal lines correspond to $\pm1\sigma$, $\pm2\sigma$ and $\pm3\sigma$.

-1 for stations POFI, MIDA, INTR, RNI2, GIUL and larger than 1 for station MPAG.

Finally, to highlight the benefits from using site-specific amplification attributes, Fig. 7 shows the PGV predictions from PD for the validation data set D_{val} but without considering the $\delta P2S$ adjustments. In this case, ϕ_{P2S} is moved back to the aleatory variability, and $\sigma = \sqrt{\sigma_{SS}^2 + \phi_{P2S}^2}$ is considered to normalize the residuals. In this case, the variability is $\sigma = 0.356$ and 0.203 for PD and IV2, respectively. As shown in Fig. 7, the spread of γ_{es} significantly increases with respect to Fig. 6. In particular, the standard deviation of γ_{es} increases from 0.09 to 0.25, as shown by the histograms of the residuals reported in Fig. 8 (first and second panel from the top). Fig. 8 also shows the distribution of the residuals between the observed and predicted Log(PGV) values (i.e. eq. (4) but without considering $\delta P2S$) predicted by different models proposed in literature (see Table 3): the (Wu *et al.* 2007) model was derived merging data from Taiwan and southern California; the model of (Zollo *et al.* 2010) was calibrated over a data set including recordings from Taiwan, California and Italy; finally, the model of (Caruso *et al.* 2017) has been recently derived from 128 Italian earthquakes. Fig. 8 shows that all models that not account for site-specific amplification term show a similar large spread of the residual distribution. It is worth warning the readers interested in operating on-site EEW systems that the use of models calibrated for regions different from the target area could also show significant offsets. This behavior is partly attributable to the use of these latter models outside their range of applicability. We conclude that the use of the site terms $\delta P2S$ both reduces the (apparent) aleatory variability of the PGV (σ_{SS} against σ), and improves the accuracy of the site-specific median predictions for most stations. The implications of these results are further argued in the discussions.

6 APPLICATION TO NEW EARTHQUAKES AND STATIONS

Besides the assessment of the predictive power of the models presented so far, in the following we consider the situation where an EEW operator would like to apply the $PD\,to\,PGV$ and $IV2\,to\,PGV$ models to a station for which the $\delta P2S$ adjustment is not known. This situation mimics the application of the on-site EEW models to stations installed after (or not considered in) the calibration phase. The data set D_{app} used in this analysis contains recordings from 37 stations and 443 events both independent from D_{cal}. Our analysis of D_{app} is intended to demonstrate the number of small to moderate earthquakes need to calibrate $\delta P2S$ when a new station has been installed in an EEW network. To estimate the $\delta P2S$ of these stations, we follow the same approach proposed by (Rodríguez-Marek *et al.* 2013; Kotha *et al.* 2017) for determining the $\delta P2S$ values within the framework of site-specific hazard assessment. The approach consists in the computation of δB_e and $\delta P2S_s$ by distributing the event-specific and site-specific residuals among the earthquake and station populations in a way similar to the random effect regression:

$$\delta B_e = \frac{\tau^2 \sum_{i=1}^{N_e} (Log(PGV_{ei}^{obs}) - Log(PGV_{ei}^{pred}))}{N_e\tau^2 + \phi_{P2S}^2 + \phi_{SS}^2} \quad (6)$$

$$\delta P2S_s = \frac{\phi_{P2S}^2 \sum_{i=1}^{N_s} (Log(PGV_{is}^{obs}) - Log(PGV_{is}^{pred}) - \delta B_e)}{N_s\phi_{P2S}^2 + \tau^2 + \phi_{SS}^2}, \quad (7)$$

where N_e and N_s are the number of recordings for event e and station s, respectively. The estimated $\delta P2S$ values are shown in Fig. 9. These values, along with the median predictions obtained using the models in Table 2 , allow us to perform site-specific predictions for the stations installed after the calibration phase. For each station, the $\delta P2S$ values in Fig. 9 were computed using all available recordings in D_{app}. These recordings are also used to evaluate the variability of $\delta P2S$ as function of the number of used recordings. Fig. 10 shows the example of station *AMT* (other examples are shown in Fig. A3 of the Appendix). Since D_{app} is composed of the recordings of the 2016–2017 central Italy sequence, for which the earthquakes show spatial and temporal clustering (Barani *et al.* 2017, 2018), the actual temporal order of occurrence of the recordings could show a large path-correlation among elements close located in the temporal

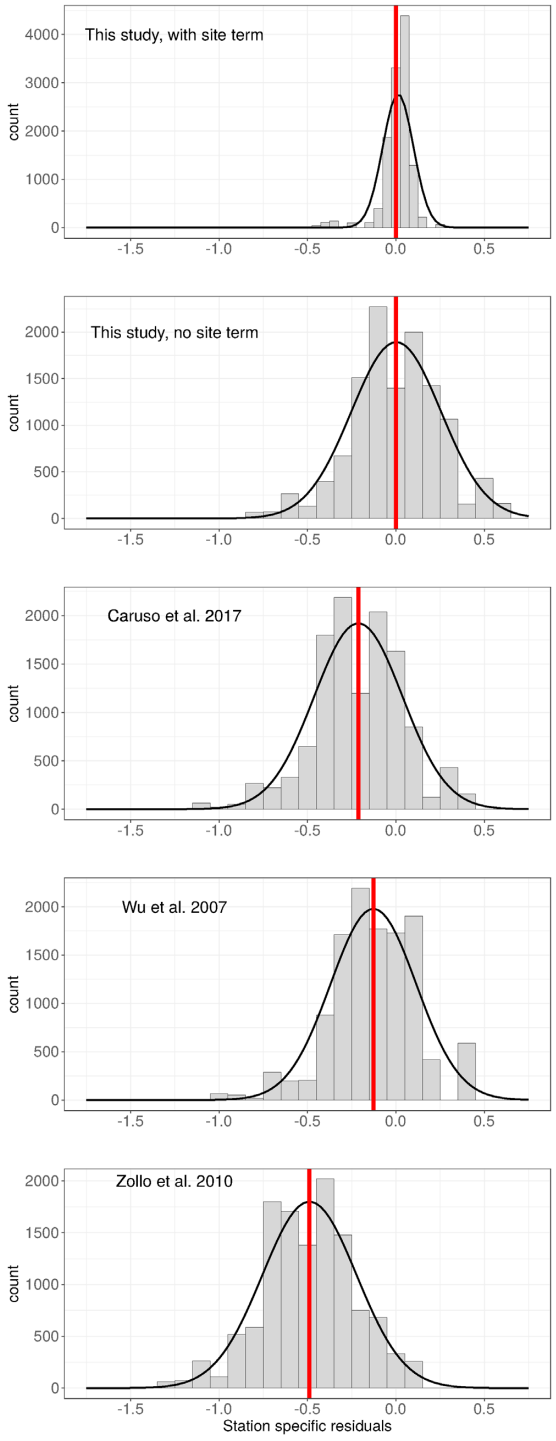

Figure 8. Histograms of γ_{es} for D_{cal} computed considering *PD* as proxy. From top to bottom: model calibrated in this study considering $\delta P2S$, without considering $\delta P2S$, model of (Caruso *et al.* 2017), model of (Wu *et al.* 2007) and model of (Zollo *et al.* 2010). The mean residual is indicated by the red vertical line, and the normal distributions with mean and standard deviation computed from each histogram are shown in black.

Table 3. Coefficients of earlier on-site EEW models.

Model	Proxy	Intercept	Slope	σ
(Caruso *et al.* 2017)	PD	1.45	0.84	0.36
(Zollo *et al.* 2010)	PD	1.30	0.73	0.36
(Wu *et al.* 2007)	PD	1.609	0.903	0.309

sequence. Therefore, we assess $\delta P2S$ for the new stations considering both the actual time order of the recordings and a shuffled version of the temporal sequence where the order of occurrence of the events has been randomized. Fig. 10 exemplifies the results for station *AMT*, whereas other examples are given in Fig. A3 of the Appendix. In these Figures, we compare the variation of $\delta P2S$ obtained considering the actual temporal order (black symbols) with those resulting from the shuffled temporal sequence (red symbols). Some stations, and mainly for PD, show a faster rate of convergence for the randomized temporal order, suggesting that the minimum number of recordings needed to get a reliable assessment of $\delta P2S$ should take into the amount of independent information carried by each new recording. Considering the random sampling in time, the convergence requires a number of recordings that varies from station to station and is on the order of a few tens (between 20 and 60).

Finally, to test the reliability of $\delta P2S$ computed through eq. (7), we apply the leave-one-out (LOO) approach (Stone 1974) to each of the 94 stations in D_{val} for which $\delta P2S$ is known from the calibration phase. Following the LOO approach, the regression is repeated by removing one station at a time from D_{cal}. The obtained model is therefore independent from the removed station, and the recordings in D_{val} are in turn used to compute the leave-one-out estimate of $\delta P2S$, by using eq. (7). The procedure is repeated until each one of the 94 stations in D_{cal} has been removed once. The results in Fig. 11 show that the stations deviating by more than $\pm 1\tilde{\phi}_{SS}$ (see Table 2) are those already pointed out in the validation section (i.e. the stations in the tails of the distributions in Fig. 7). For these stations, the $\delta P2S$ values obtained in the calibration phase do not allow predicting PGV as well as for other stations suggesting that either the median model is less suitable for describing the *PD-to-PGV* relationship (e.g. due due significant dependence on distance, azimuth or magnitude) or the $\delta S2S$ values do not fully describe their site effects. Since, for these stations, the $\delta P2S$ values obtained from the LOO approach are derived directly from the station-specific residuals (see the numerator in eq. 7), a discrepancy between the estimates of $\delta P2S$ obtained in the calibration and validation phases larger than for other stations was expected. Except for these few stations, an overall good agreement is observed, confirming the reliability of the $\delta P2S$ values.

7 DISCUSSIONS

In the framework of on-site EEW, alert protocols are defined in terms of threshold values for the ground shaking parameter of interest, such as the peak ground velocity (PGV). The expected PGV is predicted by applying empirical relationships defined for proxies computed over the early *P* waves, such as peak displacement (PD), and the integral of squared velocity (IV2). The selection of the threshold values is driven by the application of interest such as, for example, the expected level of damage suffered by the target when exposed to different shaking levels. The main results of this study is summarized in Fig. 8 which shows that the non-ergodic EEW model better predicts the site-specific PGV, with a significant reduction of the standard deviation when site amplification effects are considered. Keeping in mind that the final goal of an on-site EEW is the operational real-time prediction of the *S*-wave ground motion level at a target site in order to trigger seismic risk mitigation actions, it is worth noting that the performance of such systems (i.e., measured in terms of correct, false and missed alerts) strongly depends on the standard deviation of the adopted model. Reducing

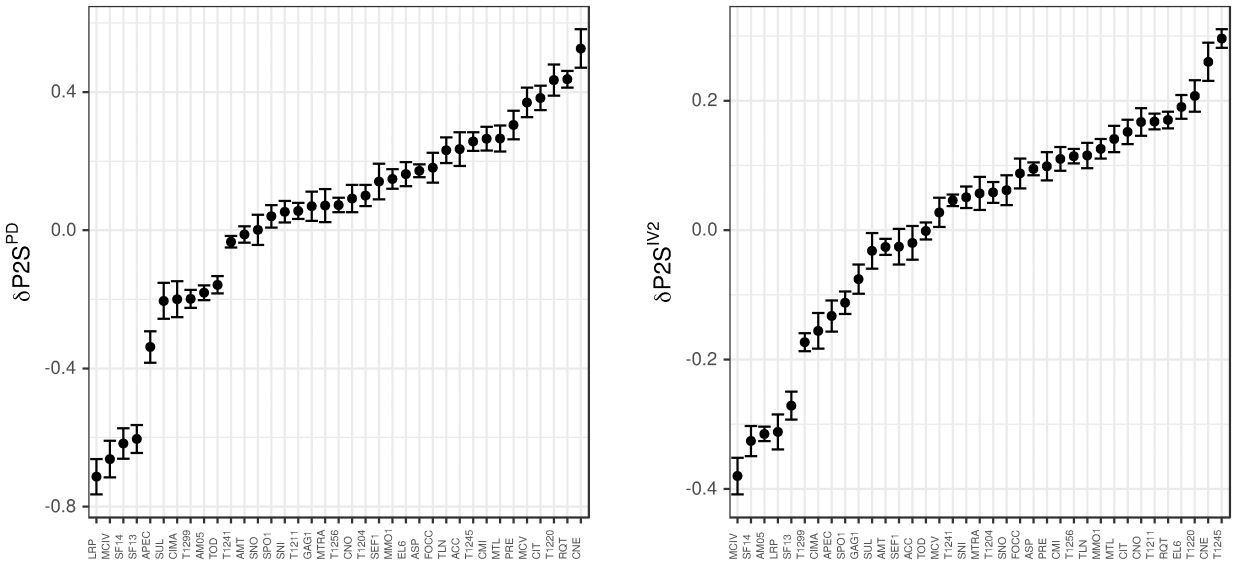

Figure 9. $\delta P2S$ for stations in D_{app}, computed following (Rodríguez-Marek *et al.* 2013; Kotha *et al.* 2017) (see eqs 6 and 7). Left: results obtained considering PD as proxy; right: results considering IV2. Symbols are color coded according to the number of recordings available for each station. Please note the different scales on the y-axes and the different station order on the x-axes.

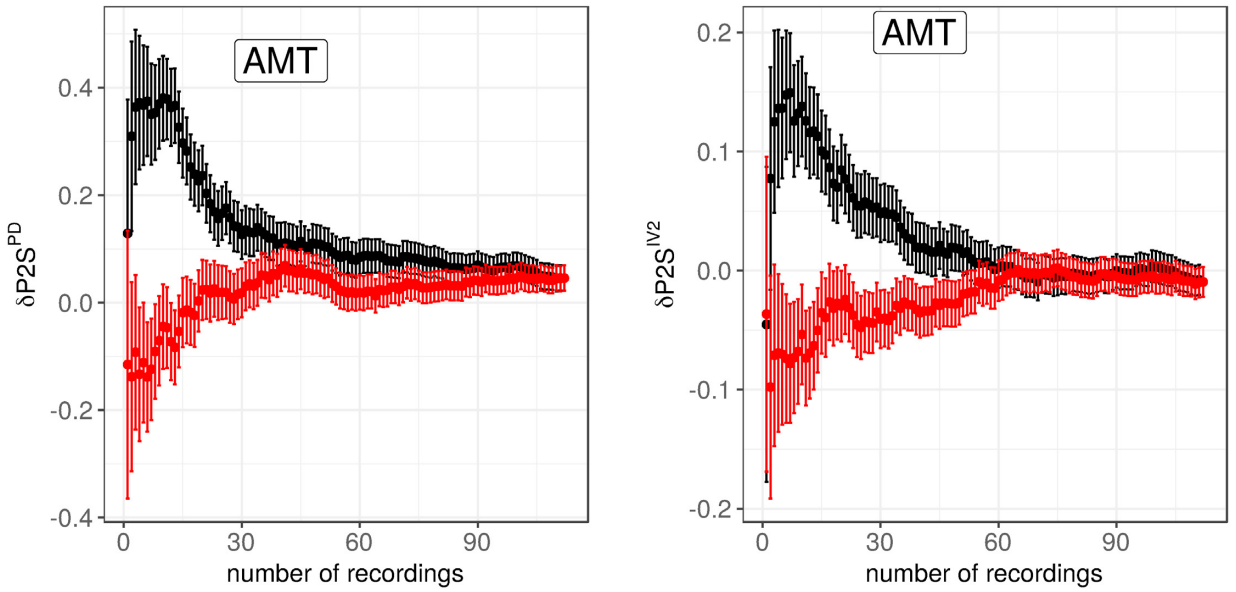

Figure 10. $\delta P2S$ for station AMT as function of the number of recordings in D_{app}, computed using eq. (7). Results obtained considering PD are shown on the left, for IV2 on the right. The results in black are obtained preserving the temporal order of the earthquakes where the results in red are obtained by randomizing the order of the events. Please note the different scales on the y-axes.

the standard deviation through a partially non-ergodic approach that take into account site effects provides a significant contribution at improving the performance of on-site EEW systems. Moreover, Fig. 8 shows that the application to our target area in central Italy of models exported from other hosting regions can generate significant bias in the mean residual. Although more detailed analysis are needed to reveal the origin of such a bias (e.g., its connection with differences in the calibration and application ranges of the involved variables), Fig. 8 warns EEW operators against including in their systems hosting models without evaluating the need of regional adjustments for the area of interest.

Turning to the details of our results, the development of empirical on-site EEW models that account for site-specific effects allows us to improve the accuracy of the expected PGV and to reduce its aleatory variability. Considering PD and accounting for site effects,the (apparent) aleatory variability of the logarithm of PGV is reduced from 0.31-0.36, typical values for ergodic on-site EEW models, to about 0.25. Interestingly, a lower variability of 0.15

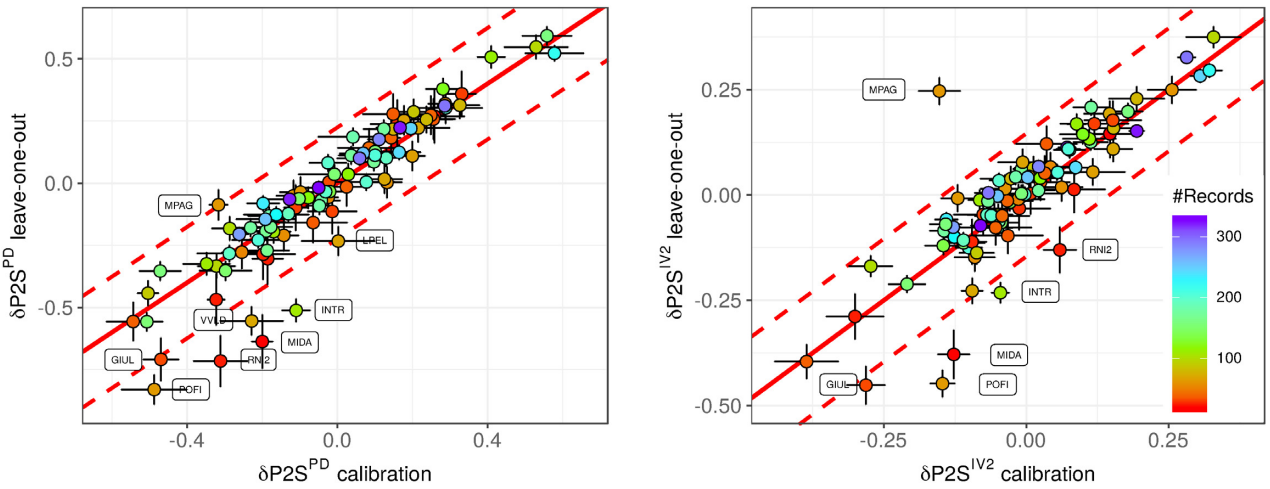

Figure 11. Results of the leave-one-out analysis: comparison between $\delta P2S$ from calibration and computed by applying equations 7 to the station left out. Left: results obtained for PD; right: results for IV2. The 1:1 line (continuous red) and $\pm\phi_{SS}$ (dashed red) are given for reference.

is obtained by considering IV2 as proxy, which suggests further consideration of this parameter for the design of on-site EEW systems. Since matrices adopted for alert systems are constructed over the expected peak shaking values and their uncertainties (Parolai *et al.* 2015), the results summarized in Fig. 8 support the adoption of a non-ergodic approach to on-site EEW. The reduction of the aleatory variability is achieved by removing the site-specific contribution from the total variance, i.e., by accounting for site amplifications through the $\delta P2S$ term (eqs 1 and 2) in the median PGV prediction. The epistemic uncertainty in $\delta P2S$ (see Fig. 3) decreases with the square root of the number of available recordings and can be treated, along with the epistemic uncertainty affecting $\phi_{SS,s}$, in the same fashion as in non-ergodic probabilistic seismic hazard assessment (Faccioli *et al.* 2015; Kotha *et al.* 2017).

Considering that the number of operational EEW systems is expanding with time, and that regions where targets and seismic threats are close located require adopting on-site approaches, we faced the problem of evaluating the number of recordings needed to assess the site amplification terms for new installed stations. To do this, we followed the approach used for non-ergodic PSHA (Kotha *et al.* 2017), where the $\delta P2S$ for the new installations can be initially set to zero, with standard error on $\delta P2S$ equal to ϕ_{P2S} (Abrahamson & Hollenback 2012). Then, with the increasing number of recordings at the station, the assessment can be refined using eq. (7). Figs 10 and A3 of the Appendix show that the number of recordings needed to achieve a stable $\delta P2S$ value varies from station to station and it is of the order of 20–60. It is therefore possible to include new installations in the network of stations for on-site EEW without requiring a re-calibration of the models. It is worth noting that as site effects we primarily mean the effect of subsurface geology on ground shaking, but they also account for the response of the hosting structure. This is an important aspect to account for, as on-site installations are often performed within buildings or infrastructure (Picozzi 2012; Parolai *et al.* 2015; Petrovic & Parolai 2016). Moreover, $\delta P2S$ also reflects possible ground motion amplification along the vertical component (i.e. affecting the predictive proxies). Indeed, we have observed a good correlation between $\delta P2S$ and the amplifications displayed by the H/V curves.

8 CONCLUSIONS

A large data set of seismic recordings allowed the calibration and validation of partially non-ergodic on-site EEW models in central Italy. As on-site early warning applications are inherently site-specific, introducing a non-ergodic perspective allows improving the accuracy of the predicted PGV and reducing the (apparent) aleatory variability of the residuals. The main conclusions drawn by this study are the following:

(1) using the peak displacement PD as predictive proxy, the incorporation of site effects reduces the variability of the logarithm of PGV from values in the range 0.31–0.36 (typical of ergodic on-site EEW models) to 0.25, being about 0.22 the contribution of the single-station variability;

(2) considering the integral of the squared velocity IV2, a lower non-ergodic variability is obtained, of the order of 0.15, which suggests further consideration of this parameter for the design of on-site EEW systems;

(3) biases in the mean residuals are observed when models calibrated for other regions, or using different data sets, are used;

(4) for stations that are not considered in the calibration phase, the site specific adjustments can be estimated and updated using newly recorded earthquakes; the number of recordings needed to achieve a stable estimate varies from station to station, and is in the range between 20 and 60;

In conclusion, adopting a partially non-ergodic perspective to on-site EEW allows us to enter more accurate and precise predictions into the alert matrices for automatic actions, taking into consideration site specific modifications to ground shaking due to local geological conditions, or to the interaction with the housing structure.

ACKNOWLEDGEMENTS

This work has been partially funded by the H2020 European project Seismology and Earthquake Engineering Research Infrastructure Alliance for Europe (SERA, http://www.sera-eu.org). All the authors contributed to the design of the study and shared the manuscript preparation. D. Spallarossa compiled the data set and processed the data to create the input tables for the regressions. The

derivation of the models was performed by D. Bindi using R software (R Development Core Team 2008). Fig. A1 was prepared with Generic Mapping Tool (Wessel *et al.* 2013). Comments and suggestions from two anonymous Reviewers and the Editor are strongly acknowledged.

REFERENCES

Abrahamson, N.A. & Hollenback, J.C., 2012. Application of single-site sigma ground motion prediction equations in practice, Paper No. 2536, in *Proceedings 15th World Conference on Earthquake Engineering,* pp. 24–28 Lisbon, Portugal.

Akinci, A., Malagnini, L. & Sabetta, F., 2010. Characteristics of the strong ground motions from the 6 April 2009 LAquila earthquake, Italy, *Soil Dyn. Earth. Eng.,* **30,** 320–355.

Al Atik, L., Abrahamson, N., Bommer, J.J., Scherbaum, F., Cotton, F. & Kuehn, N., 2010. The variability of ground-motion prediction models and its components, *Seimsol. Res. Lett.,* **81**(5), 794–801.

Anderson, J.G. & Brune, J.N., 1999. Probabilistic seismic hazard analysis without the ergodic assumption, *Seismsol. Res. Lett.,* **70,** 19–28.

Atkinson, G., 2006. Single-station sigma, *Bull. seism. Soc. Am.,* **96,** 446–455.

Barani, S., Mascandola, C., Serpelloni, E., Ferretti, G., Massa, M. & Spallarossa, D., 2017. TimeSpace evolution of seismic strain release in the area shocked by the August 24 October 30 Central Italy Seismic Sequence, *Pure appl. Geophys.,* **174,** 1875–1887.

Barani, S., Mascandola, C., Riccomagno, E., Spallarossa, D., Albarello Ferretti, G., Scafidi, S., Augliera, P. & Massa, Marco, 2018. Long-range dependence in earthquake-moment release and implications for earthquake occurrence probability, *Scient. Rep.,* **8**.

Bates, D., Mächler, M., Bolker, B. & Walker, S., 2015. Fitting linear mixed-effects models using lme4, *J. Stat. Software.,* **67,** 1–48.

Bindi, D., Iervolino, I. & Parolai, S., 2016. On-site structure-specific real-time risk assessment: perspectives from the REAKT project, *Bull. Earthq. Eng.,* **14**(9), 2471–2493.

Bindi, D., Spallarossa, D., Picozzi, M., Scafidi, D. & Cotton, F., 2018. Impact of magnitude selection on aleatory variability associated with ground-motion prediction equations: Part I: local, energy, and moment magnitude calibration and stress-drop variability in Central Italy, *Bull. seism. Soc. Am.,* **108**(3A), 1427–1441.

Böse, M., Hauksson, E., Solanki, K., Kanamori, H. & Heaton, T.H., 2009. Real-time testing of the on-site warning algorithm in Southern California and its performance during the July 29 2008 Mw5.4 Chino Hills earthquake, *Geophys. Res. Lett.,* **36,** L00B03, doi:10.1029/2008GL036366.

Brondi, P., Picozzi, M., Emolo, E., Zollo, A. & Mucciarelli, M., 2015. Predicting the macroseismic intensity from early radiated P wave energy for on-site earthquake early warning in Italy, *J. geophys. Res.: Solid Earth,* **120,** 7174–7189.

Caruso, A., Colombelli, S., Elia, L., Picozzi, M. & Zollo, A., 2017. An on-site alert level early warning system for Italy, *J. geophys. Res.: Solid Earth,* **122,** 2106–2118.

CEN, 2004. Eurocode 8: Design of structures for earthquake resistance - Part 1: general rules, seismic actions and rules for buildings, *Eur. Standard EN 1998-1:2004*.

Chiaraluce, L. *et al.*, 2017. The 2016 Central Italy seismic sequence: a first look at the mainshocks, aftershocks, and source models, *Seismol. Res. Lett.,* **88**.

Colombelli, S., Caruso, A., Zollo, A., Festa, G. & Kanamori, H., 2015. A P wave-based, on-site method for earthquake early warning, *Geophys. Res. Lett.,* **42,** 1390–1398.

Cultrera, G., Rovelli, A., Mele, G., Azzara, R., Caserta, A. & Marra, F., 2003. Azimuth dependent amplification of weak and strong ground motions within a fault zone (Nocera Umbra, Central Italy), *J. geophys. Res.,* **108**(B3), 2156.

Di Giulio, G., Rovelli, A., Cara, F., Azzara, R.M., Marra, F., Basili, R. & Caserta, A., 2003. Longduration asynchronous ground motions in the Colfiorito plain, central Italy, observed on a twodimensional dense array, *J. geophys. Res.,* **108**(B10) 2486.

Faccioli, E., Paolucci, R. & Vanini, M., 2015. Evaluation of Probabilistic Site-Specific seismic- hazard methods and associated uncertainties, with applications in the Po Plain, Northern Italy, *Bull. seism. Soc. Am.,* **105,** 2787–2807.

Festa, G., Zollo, A. & Lancieri, M., 2008. Earthquake magnitude estimation from early radiated energy, *Geophys. Res. Lett.,* **35,** L22307, doi:10.1029/2008GL035576.

Kanamori, H., 2005. Real-time seismology and earthquake damage mitigation, *Ann. Rev. Earth planet. Sci.,* **33,** 195–214.

Kotha, S.R., Bindi, D. & Cotton, F., 2017. From ergodic to region- and site-specific probabilistic seismic hazard assessment: method development and application at European and Middle Eastern sites, *Earthq. Spectra,* **33,** 1433–53.

Lermo, J. & Chávez-García., F.J., 1993. Site effect evaluation using spectral ratios with only one station, *Bull. seism. Soc. Am.,* **83**(5), 1574–1594.

Luzi, L., Hailemikael, S., Bindi, D., Pacor, F., Mele, F. & Sabetta, F., 2008. ITACA (ITalian ACcelerometric Archive): a web portal for the dissemination of Italian strong-motion data, *Seismol. Res. Lett.,* **79**(5), 716–722.

Paolucci, R., Pacor, F., Puglia, R., Ameri, G., Cauzzi, C. & Massa, M., 2011. Record processing in ITACA, the new Italian strong motion databasein Akkar, S., Gulkan, P. & Van Eck, T., eds *Earthquake Data in Engineering Seismology, Geotechnical, Geological and Earthquake Engineering Series,* Vol. **14,** p. 99113, Springer.

Parolai, S. & Richwalski, S.M., 2004. The importance of converted waves in comparing H/V and RSM site response estimates, *Bull. seism. Soc. Am.,* **94**(1), 304–313.

Parolai, S., Bindi, D., Boxberger, T., Milkereit, C., Fleming, K. & Pittore, M., 2015. OnSite early warning and rapid damage forecasting using single stations: outcomes from the REAKT project, *Seim. Res. Lett.,* **86,** 1393–1404.

Petrovic, B. & Parolai, S., 2016. Joint deconvolution of building and downhole strong-motion recordings: evidence for the seismic wavefield being radiated back into the shallow geological layers, *Bull. seism. Soc. Am.,* **106**(4).

Picozzi, M., 2012. An attempt of real-time structural response assessment by an interferometric approach: a tailor-made earthquake early warning for buildings, *Soil Dyn. Earthq. Eng.,* **38,** 109–118.

Picozzi, M., Zollo, A., Brondi, P., Colombelli, S., Elia, L. & Martino, C., 2015. Exploring the feasibility of a nationwide earthquake early warning system in Italy, *J. geophys. Res.: Solid Earth,* **120**.

Picozzi, M., Bindi, D., Brondi, P., Di Giacomo, D., Parolai, S. & Zollo, A., 2017. Rapid determination of P-wave-based Energy Magnitude: Insights on source parameter scaling of the 2016 Central Italy earthquake sequence, *Geophys. Res. Lett.,* **44**.

Pinheiro, J.C. & Bates, D.M., 2000. *Mixed-Effects Models in S and S-Plus,* Springer-Verlag, pp. 57–96.

Rodríguez-Marek, A., Cotton, F., Abrahamson, N.A., Akkar, S., Al Atik, L., Edwards, B., Montalva, G.A. & Dawood, H., 2013. A model for single-station standard deviation using data from various tectonic regions, *Bull. seism. Soc. Am.,* **103,** 3149–3163.

R Development Core Team, 2008. R: A language and environment for stat- istical computing, R Foundation for Statistical Computing, Vienna, Austria.Available at https://www.r-project.org/(last accessed June 2018).

Rovelli, A., Caserta, A., Marra, F. & Ruggiero, V., 2002. Can seismic waves be trapped inside an inactive fault zone? The case study of Nocera Umbra, Central Italy, *Bull. seism. Soc. Am.,* **92,** 2217–2232.

Satriano, C., Wu, Y.-M., Zollo, A. & Kanamori, H., 2011. Earthquake early warning: concepts, methods and physical grounds, *Soil Dyn. Earthquake Eng.,* **31,** 106–118.

Stone, M., 1974. Cross-validatory choice and assessment of statistical predictions (with discussion), *J. R. Stat. Soc., Ser. B*, **36**, 111–147.

Wang, J.P. & Wu, Y-H., 2014. Epistemic uncertainty in on-site earthquake early warning on the use of PGVPD3 empirical models, *Soil Dyn. Earthq. Eng.,* **65,** 126–130.

Wessel, P., Smith, W.H.F., Scharroo, R., Luis, J.F. & Wobbe, F., 2013. Generic mapping tools: improved version released, *EOS, Trans. Am. geohys. Un.,* **94,** 409–410.

Wu, Y.-M. & Kanamori, H., 2005. Rapid assessment of damage potential of earthquakes in Taiwan from the beginning of P waves, *Bull. seism. Soc. Am.,* **95**(3), 1181–1185.

Wu, Y.M., Yen, H.Y., Zhao, L., Huang, B.S. & Liang, W.T., 2006. Magnitude determination using initial P waves: a single-station approach, *Geophys. Res. Lett.,* **33,** L05306, doi:10.1029/2005GL025395.

Wu, Y.-M., Kanamori, H., Allen, R.M. & Hauksson, E., 2007. Determination of earthquake early warning parameters,τ_c and *Pd*, for southern California, *Geophys. J. Int.,* **170,** 711–717.

Wu, Y.M. & Kanamori, H., 2008. Development of an earthquake early warning system using real-time strong motion signals, *Sensors,* **8**(1), 1–9.

Zollo, A., Lancieri, M. & Nielsen, S., 2006. Earthquake magnitude estimation from peak amplitudes of very early seismic signals on strong motion records, *Geophys. Res. Lett.,* **33,** L23312, doi:10.1029/2006GL027795.

Zollo, A., Amoroso, O., Lancieri, M., Wu, Y.-M. & Kanamori, H., 2010. A threshold-based earthquake early warning using dense accelerometer networks, *Geophys. J Int.,* **183,** 963974.

Kanamori, H., Mori, J., Hauksson, E., Heaton, T. H., Hutton, K. & Jones, L. M., 1993. Determination of earthquake energy release and ML using TERRAscope, *Bull. Seism. Soc. Am.,* **83,** 330–346.

APPENDIX

The Appendix includes three Figures and one Table. Fig. A1 shows the maps with station locations and source-to-station ray paths for the three considered data sets (i.e. D_{cal}, D_{val} and D_{app}); Fig. A2 shows the residuals ϵ_{es}^{IV2} normalized to ϕ_{SS}, along with the single station mean normalized residual and normalized single station variability $\phi_{SS,s}/\phi_{SS}$; Fig. A3 shows the δ_{P2S} for nine stations as function of the number of considered recordings (see also Fig. 10 of the main article); finally, Table A1 lists the δ_{P2S} for PD and IV2 for the calibration stations.

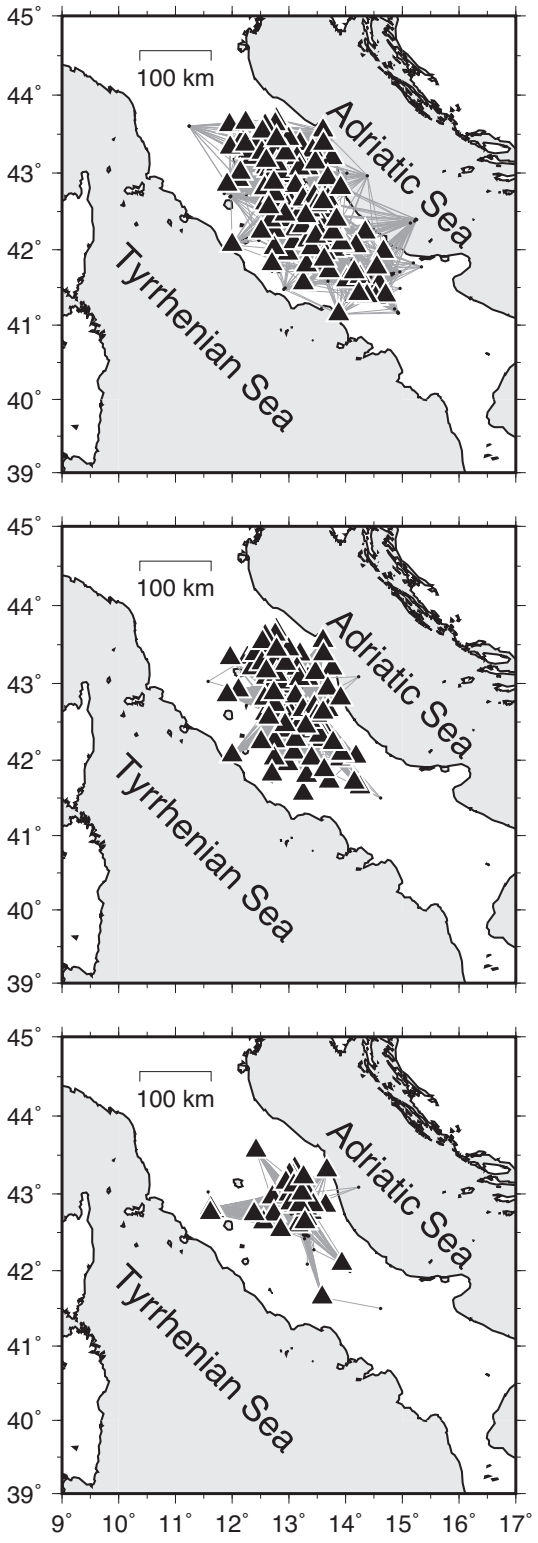

Figure A1. Data sets used in this study. Top: D_{cal}; middle: D_{val}; bottom: D_{app}. Triangles indicate the station locations; grey lines connect the station locations with epicenters.

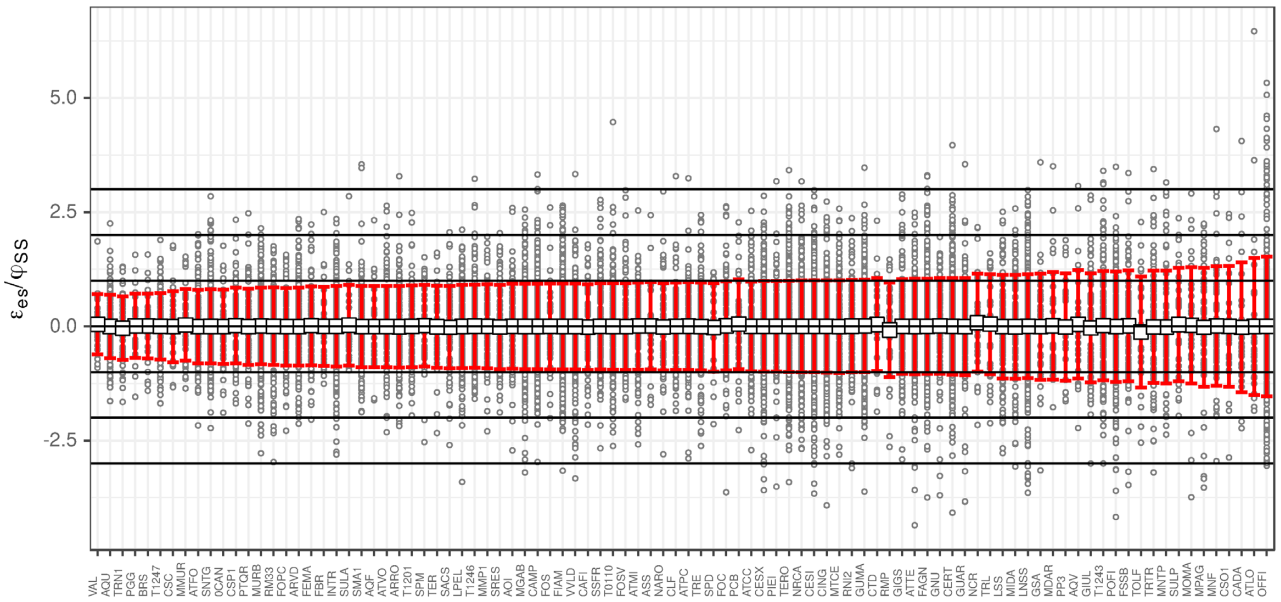

Figure A2. Residuals ϵ_{es}^{IV2} normalized to ϕ_{SS} (circles) grouped for stations in D_{cal}. For each station, the mean normalized residual (white square) and the normalized single-station variability $\phi_{SS,s}/\phi_{SS}$ (vertical red bars) are shown.

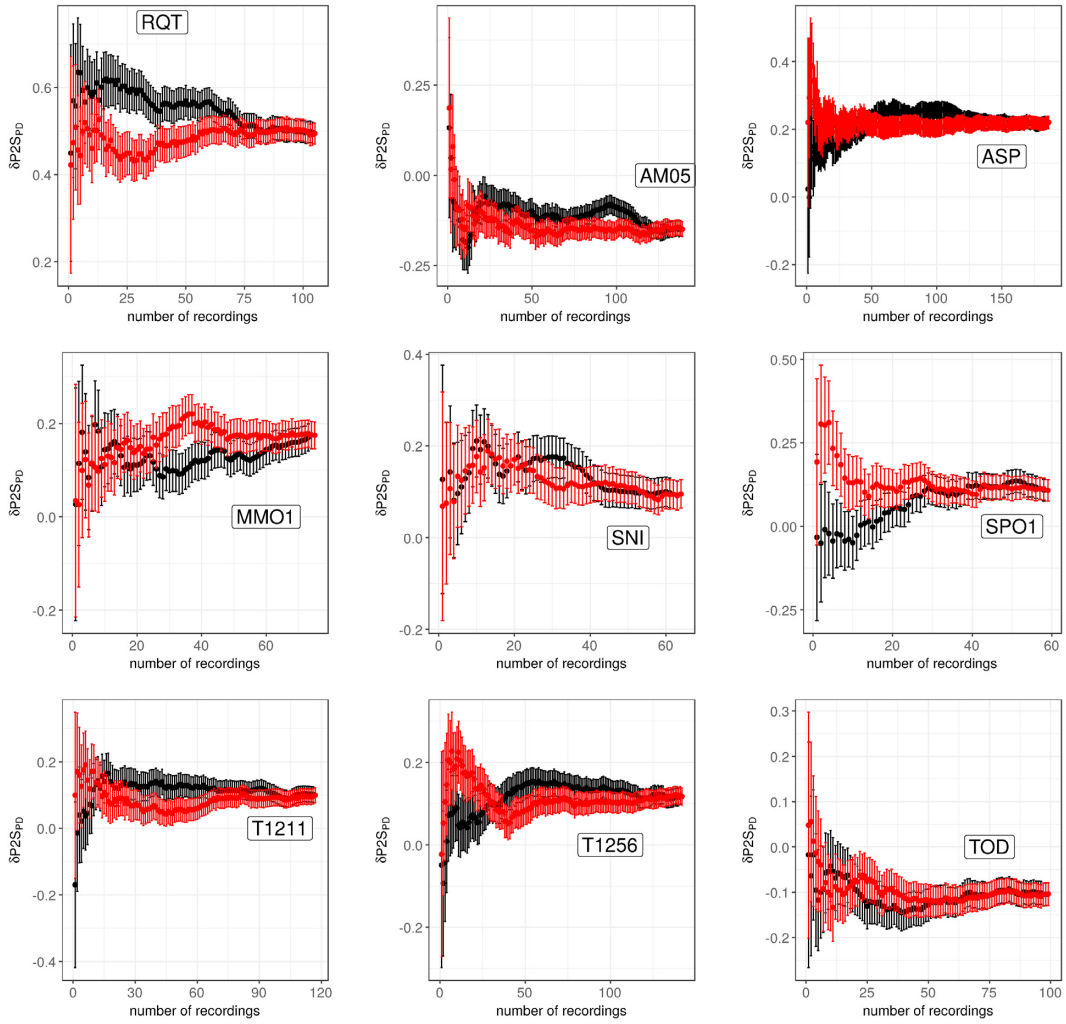

Figure A3. $\delta P2S$ for nine stations not considered in the model calibration, as function of the number of recordings in D_{app}. The values are relevant to the model for PD and are computed using eq. (7). The results in black are obtained preserving the temporal order of the earthquakes where the results in red are obtained by randomizing the order of the events. Please note the different scales on the y-axes.

Table A1. Staton-to-station residuals $\delta P2S$ (eqs 1 and 2) and 95 per cent confidence interval (CI).

Station	$\delta P2S_{PD}$	95% CI	$\delta P2S_{IV2}$	95% CI
0CAN	−0.1169	0.0670	−0.0372	0.0435
ANT	0.1163	0.0784	0.0739	0.0508
AOI	−0.1700	0.0509	−0.0060	0.0330
AQF	0.1596	0.0848	−0.0125	0.0549
AQG	0.2497	0.0917	0.1719	0.0593
AQU	−0.1839	0.0389	−0.0287	0.0251
AQV	0.2586	0.0834	0.1467	0.0540
ARRO	−0.2307	0.0396	−0.1445	0.0256
ARVD	−0.1976	0.0320	−0.1403	0.0205
ASS	0.1485	0.0833	0.0354	0.0540
ASSB	−0.0365	0.0350	−0.0421	0.0225
ATCC	−0.0081	0.0395	0.0053	0.0254
ATFO	−0.2108	0.0373	−0.1010	0.0240
ATLO	−0.2545	0.0717	−0.0140	0.0464
ATMC	−0.1281	0.0722	0.0393	0.0466
ATMI	−0.1901	0.0438	0.0759	0.0283
ATPC	−0.1776	0.0460	0.0536	0.0297
ATTE	−0.3219	0.0338	−0.0492	0.0217
ATVA	−0.4098	0.0549	−0.0391	0.0355
ATVO	−0.2877	0.0415	−0.0504	0.0268
BRS	0.2553	0.0806	0.0248	0.0523
BSSO	−0.3122	0.0815	−0.1795	0.0523
CADA	−0.0139	0.0805	−0.0758	0.0522
CAFI	−0.2978	0.0591	−0.1102	0.0383
CAFR	−0.0175	0.0661	0.0531	0.0428
CAMP	−0.1627	0.0251	−0.1263	0.0159
CCT	−0.1133	0.0978	0.0640	0.0633
CERA	−0.2904	0.0482	−0.0249	0.0311
CERT	−0.1871	0.0237	−0.0085	0.0150
CESI	0.0413	0.0218	0.0273	0.0137
CESX	−0.1272	0.0247	0.0714	0.0157
CING	−0.0250	0.0270	−0.0480	0.0172
CLF	0.2031	0.0528	0.0126	0.0342
CRE	−0.1848	0.0855	−0.0044	0.0553
CSC	0.1488	0.0836	−0.0271	0.0541
CSO1	−0.1110	0.0898	0.0074	0.0582
CSP1	0.1253	0.0525	0.1525	0.0340
CTD	0.1993	0.0880	0.1168	0.0570
FAGN	0.0770	0.0246	−0.0028	0.0156
FBR	0.2870	0.0848	0.0049	0.0550
FDMO	−0.0431	0.0226	−0.0042	0.0142
FEMA	0.2371	0.0462	0.1531	0.0299
FIAM	−0.2613	0.0206	−0.1284	0.0129
FMG	0.0293	0.0982	−0.0557	0.0634
FOC	0.5578	0.0410	0.1783	0.0264
FOPC	0.1303	0.0528	−0.0693	0.0342
FOS	0.1773	0.0671	−0.0065	0.0435
FOSV	−0.1021	0.0462	−0.0439	0.0298
FRES	−0.0513	0.0972	0.0598	0.0626
FSSB	0.1235	0.0492	0.1137	0.0318
GIGS	−0.1820	0.0374	−0.0187	0.0241
GIUL	−0.4696	0.0522	−0.2816	0.0338
GNU	0.0971	0.0479	0.1131	0.0310
GSA	0.1430	0.0702	−0.0334	0.0456
GUAR	−0.1979	0.0403	−0.0953	0.0260
GUMA	0.2857	0.0252	0.2815	0.0160
INTR	−0.1098	0.0251	−0.0455	0.0159
LG02	0.0115	0.0448	−0.1052	0.0289
LG05	0.5007	0.0399	−0.0013	0.0256
LG07	0.1569	0.0482	−0.3256	0.0311
LG08	0.3686	0.0639	0.0543	0.0413
LG10	0.2729	0.0426	0.0250	0.0274
LG11	0.2744	0.0631	0.0708	0.0408
LG12	0.4885	0.0428	0.1423	0.0275
LG13	0.3488	0.0480	0.0371	0.0310
LG14	0.0414	0.0475	−0.0480	0.0307
LG15	−0.0172	0.0455	−0.1705	0.0293
LG16	0.1341	0.0392	0.0579	0.0252
LG17	0.4012	0.0388	−0.2746	0.0249

Table A1. Continued

Station	$\delta P2S_{PD}$	95% CI	$\delta P2S_{IV2}$	95% CI
LG18	0.3928	0.0429	0.1663	0.0276
LG19	0.1946	0.0537	0.1713	0.0346
LNSS	0.1668	0.0219	0.1939	0.0138
LPEL	0.0024	0.0330	−0.0558	0.0212
LSS	−0.1303	0.0422	−0.1105	0.0273
MCT	0.3522	0.0914	0.2405	0.0592
MDAR	−0.0244	0.0773	0.0423	0.0500
MGAB	−0.1918	0.0285	−0.0507	0.0182
MIDA	−0.2000	0.0440	−0.1274	0.0284
MMP1	−0.0774	0.0555	0.0243	0.0360
MMUR	0.2152	0.0702	0.1462	0.0455
MNF	0.1320	0.0583	0.0620	0.0378
MNS	−0.1345	0.0338	−0.1037	0.0217
MNTP	−0.0205	0.0507	−0.1457	0.0328
MODR	−0.2645	0.0867	−0.0494	0.0558
MOMA	0.0288	0.0728	0.1107	0.0471
MPAG	−0.3167	0.0573	−0.1527	0.0371
MTCE	−0.3482	0.0325	−0.0817	0.0209
MURB	0.1954	0.0284	0.3053	0.0181
NARO	−0.1427	0.0556	−0.0904	0.0360
NCR	0.5289	0.0749	0.3287	0.0486
NRCA	0.4095	0.0268	0.0883	0.0170
OFFI	−0.0481	0.0270	−0.0480	0.0172
ORC	0.2696	0.0786	0.1600	0.0509
PAN	−0.3241	0.0863	−0.1605	0.0559
PARC	−0.0512	0.0629	−0.0068	0.0406
PCB	0.2881	0.0664	0.2557	0.0431
PGG	0.2488	0.0864	0.0325	0.0560
PIEI	−0.0427	0.0454	0.0214	0.0293
POFI	−0.4875	0.0344	−0.1472	0.0221
PP3	−0.0646	0.0956	−0.0324	0.0619
PTQR	−0.5041	0.0476	−0.0871	0.0308
PTRJ	−0.0841	0.0920	0.0578	0.0591
RM13	0.2124	0.0511	0.3352	0.0330
RM14	0.0407	0.0604	−0.1689	0.0390
RM16	0.3898	0.0556	0.1930	0.0360
RM20	−0.0568	0.0584	0.0153	0.0377
RM24	0.2559	0.0702	0.1535	0.0454
RM33	0.1003	0.0331	0.0736	0.0212
RMP	−0.3227	0.0784	−0.3009	0.0508
RNI2	−0.3109	0.0455	0.0589	0.0293
SACR	−0.2991	0.0874	−0.0496	0.0560
SACS	−0.5072	0.0505	−0.2095	0.0327
SGG	−0.2903	0.0802	−0.0974	0.0515
SMA1	0.0369	0.0373	−0.0675	0.0240
SNTG	−0.0499	0.0264	−0.0804	0.0168
SPD	0.0243	0.0980	−0.0539	0.0633
SPM	0.2810	0.0631	0.0992	0.0409
SRES	−0.4716	0.0437	−0.1416	0.0282
SSFR	0.2880	0.0335	0.0550	0.0215
SULA	−0.1855	0.0847	0.0838	0.0549
SULP	−0.0222	0.0782	0.1519	0.0507
T0110	−0.0313	0.0320	−0.0617	0.0205
T1201	0.1007	0.0501	−0.0086	0.0324
T1243	0.5778	0.0358	0.3214	0.0230
T1246	0.1641	0.0375	0.0865	0.0241
T1247	0.0687	0.0415	0.0024	0.0268
TER	0.0843	0.0748	−0.0425	0.0486
TERO	0.1109	0.0203	0.0215	0.0127
TOLF	−0.5436	0.0866	−0.3858	0.0561
TRE	0.0591	0.0381	−0.0666	0.0245
TRIV	−0.4439	0.0680	−0.1981	0.0437
TRL	0.3261	0.0760	0.1938	0.0493
TRN1	−0.2866	0.0592	−0.2731	0.0384
TRTR	−0.0981	0.0463	−0.1205	0.0300
VAGA	−0.1221	0.0642	0.0294	0.0412
VAL	0.3311	0.0933	0.1195	0.0604
VCEL	0.0018	0.0253	0.0265	0.0161
VVLD	−0.2282	0.0301	−0.0951	0.0192